

DFNN: A Deep Fréchet Neural Network Framework for Learning Metric-Space-Valued Responses

Kyum Kim¹, Yaqing Chen^{*1}, and Paromita Dubey^{*2}

¹Rutgers University–New Brunswick

²University of Southern California

Abstract

Regression with non-Euclidean responses—e.g., probability distributions, networks, symmetric positive-definite matrices, and compositions—has become increasingly important in modern applications. In this paper, we propose deep Fréchet neural networks (DFNNs), an end-to-end deep learning framework for predicting non-Euclidean responses—which are considered as random objects in a metric space—from Euclidean predictors. Our method leverages the representation-learning power of deep neural networks (DNNs) to the task of approximating conditional Fréchet means of the response given the predictors, the metric-space analogue of conditional expectations, by minimizing a Fréchet risk. The framework is highly flexible, accommodating diverse metrics and high-dimensional predictors. We establish a universal approximation theorem for DFNNs, advancing the state-of-the-art of neural network approximation theory to general metric-space-valued responses without making model assumptions or relying on local smoothing. Empirical studies on synthetic distributional and network-valued responses, as well as a real-world application to predicting employment occupational compositions, demonstrate that DFNNs consistently outperform existing methods.

Keywords: Compositional data, Deep learning, Distributional data, End-to-end prediction, Fréchet regression, Network data, Non-Euclidean data, Random objects, Universal approximation theorem.

1 Introduction

Regression and supervised learning are central topics in statistics and machine learning. Due to advances in data acquisition technologies, modern applications across diverse disciplines increasingly involve non-Euclidean responses—e.g., probability distributions, networks, symmetric positive-definite (SPD) matrices, or compositional data—that reside in a nonlinear metric space such as a manifold rather than in an unconstrained Euclidean space, paired

^{*}Corresponding authors.

with Euclidean covariates/features. For instance, in neuroscience, there is a strong interest in understanding how brain connectivity networks evolve with demographic and clinical covariates such as age, sex, and disease status (Fair et al., 2008), and how diffusion tensors— 3×3 SPD matrices capturing local diffusion of water in the brain—change across brain development, aging, and neurodegenerative diseases (Bennett et al., 2010); in microbiome studies, researchers investigate how host features and environmental exposures shape microbial compositions (Turnbaugh et al., 2009); in economics, a key question concerns how macroeconomic factors influence the distribution of income and inequality (Jäntti and Jenkins, 2010); in drug discovery, development, and response studies using single cell transcriptomics, a central question is predicting how the single cell gene expression distribution changes under treatments varying in drug compounds, dosage levels, and exposure durations (Aissa et al., 2021); among many others. Such non-Euclidean data, often considered as random objects on metric spaces and also referred to as object data and object-oriented data (Marron and Alonso, 2014; Müller, 2016; Marron and Dryden, 2021; Dubey et al., 2024), lack the vector-space structure assumed in classical methods for Euclidean data, thereby posing fundamental challenges to learning metric-space-valued responses—in particular, even the notion of means is no longer well-defined. Conventional regression and supervised learning methods, designed for Euclidean responses and inherently reliant on Euclidean structures, fail to respect the intrinsic geometry and complexity of non-Euclidean data and thereby cannot be applied directly. The inapplicability of these conventional methods necessitate the development of regression methodologies that can predict metric-space-valued responses from Euclidean covariates (Müller, 2016).

In statistics, a number of methodologies have been developed for regression with non-Euclidean responses. One early class of approaches is extrinsic, where non-Euclidean objects are embedded into a Euclidean space using their pairwise distance matrices so that conventional regression models can then be applied (Faraway, 2014). An alternative line of work is intrinsic, which operates directly within the geometry of the response space. Examples include a Nadaraya–Watson type kernel smoothing method (Hein, 2009) and Fréchet regression approaches (Petersen and Müller, 2019; Chen and Müller, 2022; Schötz, 2022). Among the latter, global Fréchet regression extends multiple linear regression to metric-space-valued responses. This method avoids smoothing and requires no tuning parameters, but it relies on model assumptions analogous to those of classical multiple linear models. In contrast, local Fréchet regression generalizes local linear smoothing to predict metric-space-valued responses. It allows for greater flexibility in the relationship between responses and predictors, but suffers from curse of dimensionality. Overall, extrinsic methods, while being simple to implement, may distort the geometry of the metric space, and intrinsic methods, while they can respect the geometry, either rely on strong model assumptions in analogy with parametric regression, or are subject to curse of dimensionality, thereby limiting their flexibility and applicability when dealing with even moderately high-dimensional predictors.

To accommodate high-dimensional predictors in learning metric-space-valued responses, recent research has focused on adapting classical dimension reduction techniques to the Fréchet regression setting, including principal component regression (Song and Han, 2023), single index models (Ghosal et al., 2023; Bhattacharjee and Müller, 2023), and sufficient dimension reduction (Dong and Wu, 2022; Virta et al., 2022; Ying and Yu, 2022; Zhang et al., 2024; Weng et al., 2025; Ying et al., 2025). These methods, however, rely on restrictive

linearity or distributional assumptions, are sensitive to the choice of tuning parameters, or require careful construction of kernels. In contrast, [Iao et al. \(2025\)](#) propose a deep learning based approach that learns a low-dimensional manifold representation of the regression function, which is subsequently used as input in local Fréchet regression to output the prediction of the response. Consequently, their method relies on the assumption that the regression function takes values in a low-dimensional manifold of intrinsic dimension r . However, due to the curse of dimensionality inherent in local Fréchet regression—mirroring its nonparametric regression predecessors, their approach easily becomes impractical when $r > 3$.

To overcome these limitations, we propose a deep Fréchet neural network (deep FNN or DFNN) framework that directly predicts a metric-space-valued response from the input of potentially high-dimensional Euclidean predictors. The goal of the DFNN framework is to estimate the conditional Fréchet mean ([Fréchet, 1948](#)) of the response given the predictors, as defined in Eq. (1), which is the generalized notion of a conditional mean—the target of DNN regression for Euclidean responses—extended to responses in metric spaces. Compared with a classical DNN, the core innovation of a DFNN is in the output layer, whereas the input layer and hidden layers follow the same structure. Specifically, the output layer of a DFNN consists of a single node which serves as the prediction of the response in the underlying metric space. This node, as per Eq. (2), is defined as a weighted Fréchet mean of the response, where the weights are determined by the last hidden layer. Due to the intrinsic nature of (weighted) Fréchet means, the prediction of the response output by a DFNN is therefore guaranteed to reside in the metric space underlying the response. In the special case where responses are Euclidean, given the last hidden layer, the output layer in a DFNN reduces to the predicted value given by least squares estimation of a multiple linear model regressing the Euclidean response on the nodes in the last hidden layer.

The training of a DFNN is conducted by minimizing the *Fréchet risk*, defined as the mean squared distance between the responses and the output predictions. For learning Euclidean responses, we show that the prediction given by training a DFNN is equivalent to that given by training a DNN with the same architecture of hidden layers (Remark 1). We establish a universal approximation theorem for the proposed DFNN framework (Theorem 1), which shows that the conditional Fréchet mean of the metric-space-valued response given the Euclidean predictors can be approximated arbitrarily well by some DFNN. This universal approximation theorem therefore provides the theoretical underpinning for the proposed DFNN framework learning metric-space-valued responses from Euclidean predictors.

To validate the effectiveness of DFNNs, we conducted extensive experiments on synthetic data simulated in three different settings, including distributional responses, and network-valued responses, as well as a real-world application of predicting state-wise employment occupational compositions using economic, geographic, and demographic features, covering non-Euclidean responses in diverse metric spaces. Results show that DFNN constantly and significantly outperforms the existing methods across responses in different metric spaces.

In a very recent preprint, [Zhou et al. \(2025a\)](#) independently proposed a deep neural network framework for regression with metric-space-valued responses and Euclidean predictors. However, their framework is different from ours, in particular in the way how predictions of responses are structured in the output layer. Moreover, the assumptions underlying their framework are also distinct from ours—e.g., they assume the conditional Fréchet mean takes the form of a weighted Fréchet mean with the weights given by the last hidden layer of the

network, which are nonnegative and summed up to 1, and that the metric space is compact. Neither of these assumptions is required in the DFNN framework we propose. Overall, both the methodology and the theory developed in this paper are fundamentally different from those in Zhou et al. (2025a), and thus the two works have little overlap.

The remainder of the paper is organized as follows. In the rest of Section 1, we highlight the main contributions of this paper and review related work. In Section 2, we introduce the proposed DFNN framework for regression with metric-space-valued responses and Euclidean predictors. In Section 3, we establish the universal approximation theorem of DFNNs. Section 4 presents implementation details of the proposed DFNN framework and empirical experiments which demonstrate the superior prediction performance across different types of non-Euclidean responses. We conclude the paper with a discussion in Section 5.

1.1 Main Contributions

This paper focuses on deep learning-based regression with responses lying in a general metric space paired with Euclidean predictors. The main contributions are threefold.

- We propose an end-to-end deep Fréchet neural network (DFNN) framework for regression tasks with metric-space-valued responses and Euclidean predictors, which extends classical DNNs to the scope of predicting non-Euclidean responses. The DFNN framework is highly flexible, capable of accommodating diverse metric spaces and high-dimensional predictors without restricting to shallow models or parametric/semiparametric models or relying on any low-dimensional (manifold) embeddings of the regression target. The prediction of non-Euclidean responses obtained by training a DFNN respects the geometry of the response space.
- We establish a universal approximation theorem showing that DFNNs can approximate conditional Fréchet mean of the response given the predictors—the target of learning a metric-space-valued response from Euclidean predictors—arbitrarily well.
- We conduct extensive experiments, which demonstrate the superior performance of DFNNs over existing methods for predicting non-Euclidean responses from Euclidean predictors with responses lying in different metric spaces.

1.2 Related Work

Fréchet mean. The notion of Fréchet means or barycenters is a generalization of averages to random objects residing in a general metric space. It is defined as the minimizer(s) of a Fréchet functional—the expected squared distance to the random object of interest—over the corresponding metric space (Fréchet, 1948). The existence and uniqueness of Fréchet means is guaranteed for Hadamard spaces (Sturm, 2003) and have been studied for Riemannian manifolds, Wasserstein space, Alexandrov spaces, and proper metric spaces (e.g., Agueh and Carlier, 2011; Ohta, 2012; Kim and Pass, 2017; Le Gouic and Loubes, 2017). Properties including asymptotic behavior of empirical barycenters have been established for Riemannian manifolds, Wasserstein space and general metric spaces (e.g., Bhattacharya and Patrangenaru, 2002; Schötz, 2019; Zemel and Panaretos, 2019; Ahidar-Coutrix et al., 2020; Le Gouic

et al., 2022; Brunel and Serres, 2024). As an extension to a supervised setting where the metric-space-valued random object is observed along with Euclidean predictors, the question of interest is to estimate the *conditional Fréchet mean* of the random object given the predictors. Specifically, the conditional Fréchet mean is defined as the minimizer(s) of the expected squared distance to the random object conditioning on the predictors, which is the target of regression with metric-space-valued responses and Euclidean predictors (Petersen and Müller, 2019).

Fréchet regression for metric-space-valued responses. First introduced by Petersen and Müller (2019), Fréchet regression is a class of methods that aims to estimate the conditional Fréchet mean of a response lying in a metric space given Euclidean predictors. Global Fréchet regression and local Fréchet regression by can be viewed as generalizations of multiple linear models and local linear regression and uniform rates of convergence have been established for the corresponding estimators of the conditional Fréchet means (Petersen and Müller, 2019; Chen and Müller, 2022). Since then, other variants of Fréchet regression have been developed as well as methods to improve the prediction performance of global Fréchet regression (Schötz, 2020; Lin and Müller, 2021; Bhattacharjee and Müller, 2023; Ghosal et al., 2023; Song and Han, 2023; Capitaine et al., 2024; Qiu et al., 2024; Yan et al., 2024; Bhattacharjee et al., 2025; Kurisu and Otsu, 2025; Zhou et al., 2025b, among others).

Beside methodologies—such as Fréchet regression—that are developed for responses lying in a general metric space, there are also regression approaches that are specialized for a specific type of non-Euclidean responses, i.e., responses lying in a specific metric space, paired with Euclidean predictors. While they may be only applicable to one type of non-Euclidean responses, thereby lacking generality compared with methodologies developed for responses lying in a general metric space, specialized methods exploit structure of particular response spaces and hence may achieve better predictive accuracy and provide more interpretable results than approaches applicable to general metric spaces.

Regression methods for finite-dimensional Riemannian responses. The analysis of random objects taking values in a finite-dimensional differentiable Riemannian manifold, including statistics for manifold-valued data—which foster object-oriented data analysis—shape analysis, and geometric statistics, is a topic that has been extensively studied (e.g., Marron and Alonso, 2014; Dryden and Mardia, 2016; Marron and Dryden, 2021; Huckemann and Eltzner, 2021). Regression models for this type of non-Euclidean responses paired with Euclidean predictors include regression for general Riemannian responses (e.g., Davis et al., 2007; Shi et al., 2009; Hinkle et al., 2012; Cornea et al., 2017; Lin et al., 2017; Choi et al., 2025), spherical/directional regression (e.g., Fisher et al., 1987; Jupp and Kent, 1987; Chang, 1989; Prentice, 1989; Fisher, 1995; Mardia and Jupp, 2009; Di Marzio et al., 2014; Scealy and Wood, 2019), regression for SPD matrices (e.g., Zhu et al., 2009; Yuan et al., 2012; Petersen et al., 2019; Lin et al., 2023; Xu and Li, 2025), and network/graph regression (e.g., Severn et al., 2021; Calissano et al., 2022; Severn et al., 2022; Zhou and Müller, 2022; Zhou et al., 2023), among others.

Regression methods for compositional responses. Compositional data are another type of data which cannot be treated as classical Euclidean data due to the constraints that entries have to be non-negative and sum up to 1. Methods for the analysis of compositional data including regression with compositional responses have been developed mainly using Aitchison metrics including the simple pairwise log-ratio (LR), additive log-ratio (ALR), and centered log-ratio (CLR) metrics (e.g., Aitchison, 1982, 1986; Filzmoser et al., 2018; Greenacre, 2021; Greenacre et al., 2023) and geodesic metric on a (hyper)sphere applied to square root transformed compositions (e.g., Scealy and Welsh, 2011, 2017; Li et al., 2023).

Regression methods for distributional responses. Probability distributions or probability density functions are another important type of non-Euclidean data (Petersen et al., 2022). While the space of distributions is equipped with Riemannian structures under certain metrics, methods for finite-dimensional Riemannian data cannot be directly applied to the analysis of distributional data due to their infinite-dimensional nature. For regression with univariate distributional responses, existing methods include: plain vanilla methods that view density functions as elements in an \mathcal{L}_2 space—a space of square-integrable functions on certain domain (e.g., Oliva et al., 2013); transformation- or embedding-based methods, which first map distributions into an unconstrained Hilbert space using transformations including log quantile density (LQD) centered log-ratio (CLR) or kernel mean embedding so that classical functional regression methods can then be applied (van den Boogaart et al., 2014; Petersen and Müller, 2016; Hron et al., 2016; Szabó et al., 2016; Petersen et al., 2019; Han et al., 2020; Maier et al., 2025, among others); manifold-based methods, which leverages the Riemannian or pseudo-Riemannian geometries of the space of distributions endowed with the Fisher–Rao metric or 2-Wasserstein metric (Srivastava et al., 2007; Bigot et al., 2017; Cazelles et al., 2018; Ghodrati and Panaretos, 2022; Pegoraro and Beraha, 2022; Zhang et al., 2022; Chen et al., 2023; Zhu and Müller, 2023; Zhou and Müller, 2024; Zhu and Müller, 2024, among others). In addition to univariate distributional responses, regression methods have also been developed for multivariate distributional responses (Guégan and Iacopini, 2018; Chen and Müller, 2023; Okano and Imaizumi, 2023; Ghodrati and Panaretos, 2023; Hron et al., 2023; Fan and Müller, 2024; Zhu and Müller, 2024, among others).

Dimension reduction for Fréchet regression. To address the challenges posed by high-dimensional predictors in learning metric-space-valued responses, a number of works have extended classical dimension reduction techniques to the Fréchet regression setting. These include sufficient dimension reduction (Dong and Wu, 2022; Virta et al., 2022; Ying and Yu, 2022; Zhang et al., 2024; Weng et al., 2025; Ying et al., 2025), single index models (Ghosal et al., 2023; Bhattacharjee and Müller, 2023), and principal component regression (Song and Han, 2023), among others.

Deep learning based methods for regression for non-Euclidean data. Deep learning based methods developed for Euclidean data have been generalized to non-Euclidean data. Arising from representation learning for symbolic data, manifold considerations are found to be necessary to capture the structural geometry of some complex data (Nickel and Kiela, 2017). Existing work of extending deep learning based methods to regression or su-

pervised learning with non-Euclidean data mostly tackle non-Euclidean inputs. Among that, most investigations focus on a specific type of Riemannian manifolds, such as data in hyperbolic spaces (e.g., Ganea et al., 2018; Gulcehre et al., 2019; Liu et al., 2019; Chami et al., 2019; Chen et al., 2022; Peng et al., 2021), SPD matrices (e.g., Huang and Van Gool, 2017; Brooks et al., 2019; Nguyen et al., 2019; Nguyen, 2021), spherical data (e.g., Cohen et al., 2018; Coors et al., 2018; Fang et al., 2020), while representation learning has also been investigated for non-Euclidean data, in particular Riemannian data, which is often referred to as geometric (deep) learning (e.g., Masci et al., 2015; Bronstein et al., 2017; Kipf and Welling, 2017; Chakraborty et al., 2020; Sun et al., 2024). Another line of research deals with regression with manifold-valued outputs (e.g., Pan et al., 2022; Chen et al., 2023). A more recent line of work integrates representation learning into the Fréchet regression framework for responses in general metric spaces paired with Euclidean predictors. Iao et al. (2025) proposed a deep learning based method that assumes the regression function—namely, the conditional Fréchet means—resides on a low-dimensional manifold. Their approach employs a DNN to learn this manifold representations, on which local Fréchet regression is then applied to predict responses in the metric space. Nonetheless, its effectiveness relies critically on the low-dimensional manifold representation assumption on the conditional Fréchet mean, and, inherent from local Fréchet regression, it remains vulnerable to the curse of dimensionality.

Related learning frameworks for different purposes. There exist other learning frameworks that are related to the analysis of non-Euclidean data, but they—at least alone—are not methods for regression with non-Euclidean responses paired with Euclidean predictors. Examples include: manifold learning (Ghojogh et al., 2023), which can be used to embed Euclidean inputs into a low-dimensional manifold; metric learning (Bellet et al., 2015), which learns similarity/distance for a specific supervised or unsupervised task, e.g., for classification or dimension reduction.

2 DFNN: Deep Fréchet Neural Network

Let (Ω, d) be a separable metric space. Consider a random pair (\mathbf{X}, Y) with a joint distribution on the product space $\mathcal{D} \times \Omega$, where \mathcal{D} is a compact subset of \mathbb{R}^p , without loss of generality assumed to be $[0, 1]^p$ in this paper. In regression tasks, the goal is to estimate the conditional Fréchet mean of Y given $\mathbf{X} = \mathbf{x}$, denoted by $m_{\oplus}(\mathbf{x})$ for any $\mathbf{x} \in \mathcal{D}$; specifically, $m_{\oplus}(\mathbf{x})$ is defined as

$$m_{\oplus}(\mathbf{x}) = \arg \min_{\omega \in \Omega} M(\omega, \mathbf{x}) \quad \text{with } M(\omega, \mathbf{x}) = \mathbb{E}\{d^2(Y, \omega) \mid \mathbf{X} = \mathbf{x}\}. \quad (1)$$

To this end, we propose a deep Fréchet neural network (DFNN) framework which integrates global Fréchet regression (Petersen and Müller, 2019) with deep neural network structures and provides an end-to-end regression method for metric-space-valued responses paired with Euclidean predictors. Specifically, we define a DFNN with L hidden layers as follows.

Let $p_0 = p$. For each $l = 1, \dots, L$, suppose the l -th hidden layer consists of p_l nodes. Let \mathbf{W}_l be a weight matrix in $\mathbb{R}^{p_l \times p_{l-1}}$, $\mathbf{b}_l \in \mathbb{R}^{p_l}$ be a shift vector, and $\boldsymbol{\theta}_l = (\mathbf{W}_1, \mathbf{b}_1, \mathbf{W}_2, \mathbf{b}_2, \dots, \mathbf{W}_l, \mathbf{b}_l)$ be the weight matrices $\{\mathbf{W}_k\}_{k=1}^l$ and shift vectors $\{\mathbf{b}_k\}_{k=1}^l$ of the first l hidden layers, which

takes values in $\Theta_l = \mathbb{R}^{p_1 \times p_0} \times \mathbb{R}^{p_1} \times \mathbb{R}^{p_2 \times p_1} \times \mathbb{R}^{p_2} \times \cdots \times \mathbb{R}^{p_l \times p_{l-1}} \times \mathbb{R}^{p_l}$. Let $g_l(\cdot; \boldsymbol{\theta}_l): \mathbb{R}^p \rightarrow \mathbb{R}^{p_l}$ denote the map that maps the input layer of p predictors to the l -th hidden layer of p_l nodes. For any given $\{\mathbf{W}_l, \mathbf{b}_l\}_{l=1}^L$, the maps $\{g_l(\cdot; \boldsymbol{\theta}_l)\}_{l=1}^L$ can be defined in a recursive way. As an initialization, define $\boldsymbol{\theta}_0 = \emptyset$ and $g_0(\cdot; \boldsymbol{\theta}_0) = \text{id}(\cdot)$ being the identity function, i.e., $g_0(\mathbf{x}; \boldsymbol{\theta}_0) = \mathbf{x}$ for all $\mathbf{x} \in \mathbb{R}^p$. Then for each $l = 1, \dots, L$, the map $g_l(\cdot; \boldsymbol{\theta}_l)$ is defined as

$$g_l(\mathbf{x}; \boldsymbol{\theta}_l) = \sigma\{\mathbf{W}_l g_{l-1}(\mathbf{x}; \boldsymbol{\theta}_{l-1}) + \mathbf{b}_l\} \quad \text{for } \mathbf{x} \in \mathbb{R}^p,$$

where $\sigma(\cdot)$ denotes the component-wise rectifier linear unit (ReLU) activation function, i.e., $\sigma(\mathbf{a}) = (\max\{0, a_1\}, \dots, \max\{0, a_q\})^\top$ for $\mathbf{a} \in \mathbb{R}^q$ for any integer $q \geq 1$. The output layer of a DFNN is defined as a layer of a single node, denoted by $m_{\oplus}^{\text{NN}}(\mathbf{x}; \boldsymbol{\theta}_L)$, which serves as the prediction of the response:

$$\begin{aligned} m_{\oplus}^{\text{NN}}(\mathbf{x}; \boldsymbol{\theta}_L) &= \arg \min_{\omega \in \Omega} M^{\text{NN}}(\omega, \mathbf{x}; \boldsymbol{\theta}_L) \\ \text{with } M^{\text{NN}}(\omega, \mathbf{x}; \boldsymbol{\theta}_L) &= \mathbb{E} [s\{g_L(\mathbf{x}; \boldsymbol{\theta}_L), g_L(\mathbf{X}; \boldsymbol{\theta}_L)\} d^2(Y, \omega)]. \end{aligned} \quad (2)$$

Here, for any $\mathbf{x} \in \mathbb{R}^p$,

$$s\{g_L(\mathbf{x}; \boldsymbol{\theta}_L), g_L(\mathbf{X}; \boldsymbol{\theta}_L)\} = 1 + (g_L(\mathbf{x}; \boldsymbol{\theta}_L) - \boldsymbol{\mu}_{\boldsymbol{\theta}_L})^\top \boldsymbol{\Sigma}_{\boldsymbol{\theta}_L}^{-1} (g_L(\mathbf{X}; \boldsymbol{\theta}_L) - \boldsymbol{\mu}_{\boldsymbol{\theta}_L}), \quad (3)$$

with $\boldsymbol{\mu}_{\boldsymbol{\theta}_L} = \mathbb{E}\{g_L(\mathbf{X}; \boldsymbol{\theta}_L)\}$ and $\boldsymbol{\Sigma}_{\boldsymbol{\theta}_L} = \text{Cov}\{g_L(\mathbf{X}; \boldsymbol{\theta}_L)\}$, corresponds to the global Fréchet regression weights (Petersen and Müller, 2019) applied to the final hidden-layer representations $g_L(\mathbf{x}; \boldsymbol{\theta}_L)$ and $g_L(\mathbf{X}; \boldsymbol{\theta}_L)$, and $M^{\text{NN}}(\omega, \mathbf{x}; \boldsymbol{\theta}_L)$ is the global Fréchet regression objective function. At the population level, a DFNN is trained by minimizing the *Fréchet risk* $R(\boldsymbol{\theta}_L)$, which is defined as the mean squared distance between the response Y and the output layer $m_{\oplus}^{\text{NN}}(\mathbf{x}; \boldsymbol{\theta}_L)$,

$$R(\boldsymbol{\theta}_L) = \mathbb{E}\{d^2[Y, m_{\oplus}^{\text{NN}}(\mathbf{X}; \boldsymbol{\theta}_L)]\}. \quad (4)$$

Let $\boldsymbol{\theta}_L^* = \arg \min_{\boldsymbol{\theta}_L \in \Theta_L} R(\boldsymbol{\theta}_L)$. A trained DFNN predicts the response Y given $\mathbf{X} = \mathbf{x}$ by

$$\tilde{Y}(\mathbf{x}) = m_{\oplus}^{\text{NN}}(\mathbf{x}; \boldsymbol{\theta}_L^*) \quad \text{for any } \mathbf{x} \in \mathbb{R}^p. \quad (5)$$

Remark 1. For $\Omega = \mathbb{R}$ with the Euclidean metric $d = d_E$, minimizing the Fréchet risk in Eq. (4) for the DFNN output $m_{\oplus}^{\text{NN}}(\mathbf{x}; \boldsymbol{\theta}_L)$ is equivalent to minimizing the mean-squared error of a standard DNN with L hidden layers and a linear activation in the output layer. Consider a DNN with L hidden layers, a single output node ($p_{L+1} = 1$), and parameters $\boldsymbol{\theta}_{L+1} = (\mathbf{W}_1, \mathbf{b}_1, \dots, \mathbf{W}_{L+1}, \mathbf{b}_{L+1})$. In a standard DNN, with $\mathbf{W}_{L+1} \in \mathbb{R}^{1 \times p_L}$ and $\mathbf{b}_{L+1} \in \mathbb{R}$, the output node is given by

$$g_{L+1}(\mathbf{x}; \boldsymbol{\theta}_{L+1}) = \mathbf{W}_{L+1} g_L(\mathbf{x}; \boldsymbol{\theta}_L) + \mathbf{b}_{L+1} \quad \text{for } \mathbf{x} \in \mathbb{R}^p.$$

At the population level, training a DNN by minimizing the mean squared error over $\boldsymbol{\theta}_{L+1}$

can be expressed as

$$\begin{aligned}
& \min_{\boldsymbol{\theta}_{L+1}} \mathbb{E}\{Y - g_{L+1}(\mathbf{X}; \boldsymbol{\theta}_{L+1})\}^2 \\
&= \min_{\boldsymbol{\theta}_{L+1}} \mathbb{E}\{Y - \mathbf{W}_{L+1}g_L(\mathbf{x}; \boldsymbol{\theta}_L) - \mathbf{b}_{L+1}\}^2 \\
&= \min_{\boldsymbol{\theta}_L} \min_{\mathbf{W}_{L+1}, \mathbf{b}_{L+1}} \mathbb{E} [d_{\mathbb{E}}^2\{Y, \mathbf{W}_{L+1}g_L(\mathbf{x}; \boldsymbol{\theta}_L) + \mathbf{b}_{L+1}\}] \\
&= \min_{\boldsymbol{\theta}_L} \mathbb{E} \left(d_{\mathbb{E}}^2 \left\{ Y, \arg \min_{\omega \in \Omega} \mathbb{E} [s\{g_L(\mathbf{x}; \boldsymbol{\theta}_L), g_L(\mathbf{X}; \boldsymbol{\theta}_L)\} d_{\mathbb{E}}^2(Y, \omega)] \right\} \right) \\
&= \min_{\boldsymbol{\theta}_L} \mathbb{E} (d_{\mathbb{E}}^2 \{Y, m_{\oplus}^{\text{NN}}(\mathbf{X}; \boldsymbol{\theta}_L)\}),
\end{aligned} \tag{6}$$

where the third equality in Eq. (6) is implied by the global Fréchet regression formulation in Section 2.2 of Petersen and Müller (2019), with $s\{g_L(\mathbf{x}; \boldsymbol{\theta}_L), g_L(\mathbf{X}; \boldsymbol{\theta}_L)\}$ given in Eq. (3). Thus, in the Euclidean case, DFNN training by minimizing Fréchet risk coincides with standard DNN training by minimizing mean squared error.

Remark 1 shows that for scalar responses with the Euclidean metric—i.e., $\Omega = \mathbb{R}$ and $d = d_{\mathbb{E}}$ —the DFNN predictor coincides with that of a standard DNN of the same architecture with a linear activation for the output layer trained by minimizing mean squared error. Thus, the DFNN framework directly generalizes standard DNNs from scalar responses to metric-space-valued responses.

In practice, consider a random sample of n i.i.d. pairs $(\mathbf{X}_1, Y_1), \dots, (\mathbf{X}_n, Y_n)$ from the joint distribution of (\mathbf{X}, Y) on the $\mathcal{D} \times \Omega$. We define the *empirical Fréchet risk* as

$$\hat{R}_n(\boldsymbol{\theta}_L) = \frac{1}{n} \sum_{i=1}^n d^2\{Y_i, \hat{m}_{\oplus}^{\text{NN}}(\mathbf{X}_i; \boldsymbol{\theta}_L)\} \tag{7}$$

where for any $\mathbf{x} \in \mathbb{R}^p$, the empirical estimator of the DFNN output layer, $m_{\oplus}^{\text{NN}}(\mathbf{x}; \boldsymbol{\theta}_L)$, is given by:

$$\begin{aligned}
\hat{m}_{\oplus}^{\text{NN}}(\mathbf{x}; \boldsymbol{\theta}_L) &= \arg \min_{\omega \in \Omega} \hat{M}^{\text{NN}}(\omega, \mathbf{x}; \boldsymbol{\theta}_L) \\
\text{with } \hat{M}^{\text{NN}}(\omega, \mathbf{x}; \boldsymbol{\theta}_L) &= \frac{1}{n} \sum_{i=1}^n \hat{s}\{g_L(\mathbf{x}; \boldsymbol{\theta}_L), g_L(\mathbf{X}_i; \boldsymbol{\theta}_L)\} d^2(Y_i, \omega),
\end{aligned} \tag{8}$$

and the weights are estimated as:

$$\hat{s}\{g_L(\mathbf{x}; \boldsymbol{\theta}_L), g_L(\mathbf{X}_i; \boldsymbol{\theta}_L)\} = 1 + (g_L(\mathbf{x}; \boldsymbol{\theta}_L) - \hat{\boldsymbol{\mu}}_{\boldsymbol{\theta}_L})^\top \hat{\boldsymbol{\Sigma}}_{\boldsymbol{\theta}_L}^{-1} (g_L(\mathbf{X}_i; \boldsymbol{\theta}_L) - \hat{\boldsymbol{\mu}}_{\boldsymbol{\theta}_L}), \tag{9}$$

with $\hat{\boldsymbol{\mu}}_{\boldsymbol{\theta}_L} = \frac{1}{n} \sum_{i=1}^n g_L(\mathbf{X}_i; \boldsymbol{\theta}_L)$ and $\hat{\boldsymbol{\Sigma}}_{\boldsymbol{\theta}_L} = \frac{1}{n} \sum_{i=1}^n \{g_L(\mathbf{X}_i; \boldsymbol{\theta}_L) - \hat{\boldsymbol{\mu}}_{\boldsymbol{\theta}_L}\} \{g_L(\mathbf{X}_i; \boldsymbol{\theta}_L) - \hat{\boldsymbol{\mu}}_{\boldsymbol{\theta}_L}\}^\top$. Finally, the trained DFNN gives the empirical predictor $\hat{Y}(\cdot)$ given by

$$\hat{Y}(\mathbf{x}) = \hat{m}_{\oplus}^{\text{NN}}(\mathbf{x}; \hat{\boldsymbol{\theta}}_L^*) \quad \text{for any } \mathbf{x} \in \mathbb{R}^p, \tag{10}$$

where

$$\hat{\boldsymbol{\theta}}_L^* = \arg \min_{\boldsymbol{\theta}_L \in \Theta_L} \hat{R}_n(\boldsymbol{\theta}_L)$$

Algorithm 1 DFNN Training Procedure

Input: Training samples $\{(\mathbf{X}_i, Y_i)\}_{i=1}^n$

Output: Trained neural network parameters $\hat{\boldsymbol{\theta}}_L^*$

1: Initialize network parameters $\boldsymbol{\theta}_L$

2: Obtain $\hat{\boldsymbol{\theta}}_L^*$ using the SGD optimizer to minimize the *empirical Fréchet risk* $\hat{R}_n(\boldsymbol{\theta}_L)$ defined in Eq. (7).

is an *empirical Fréchet risk minimizer* over the parameter space Θ_L , which consists of the weight matrices and the shift vectors and induces the trained DFNN, and \hat{R}_n is the empirical Fréchet risk defined in Eq. (7).

In summary, the DFNN framework implements a flexible, model-agnostic way to learn conditional Fréchet means in metric spaces by minimizing the empirical Fréchet risk in Eq. (7). The construction above defines the network architecture and the associated population and empirical objectives, yet an essential theoretical question remains: *How well can DFNN approximate the true conditional Fréchet mean $m_{\oplus}(\cdot)$?* This requires a formal analysis of the approximation power of DFNNs as function approximators over metric space-valued responses. In the next section, we establish a universal approximation theorem that guarantees this property under suitable regularity conditions.

3 Theoretical Results

With the DFNN architecture and its population and empirical training objectives defined in Section 2, we next analyze the theoretical expressive power of this framework. In particular, we show that DFNNs can approximate the conditional Fréchet mean $m_{\oplus}(\cdot)$ defined in Eq. (1) arbitrarily well under mild regularity conditions. To specify the smoothness properties of $M(\omega, \mathbf{x})$ defined in Eq. (1), we consider the Sobolev spaces $\mathcal{W}^{r,\infty}(\mathcal{D})$ with $r = 1, 2, \dots$ where $\mathcal{W}^{r,\infty}(\mathcal{D})$ is defined as functions on \mathcal{D} lying in $\mathcal{L}_{\infty}(\mathcal{D})$ with $\mathcal{L}_{\infty}(\mathcal{D}) = \{f : \mathcal{D} \rightarrow \mathbb{R} : \|f\|_{\infty} < \infty\}$ and $\|f\|_{\infty} = \text{ess sup}_{\mathbf{x} \in \mathcal{D}} |f(\mathbf{x})|$, along with their weak derivatives up to order r . The Sobolev norm of a function $f \in \mathcal{W}^{r,\infty}(\mathcal{D})$ is defined as

$$\|f\|_{\mathcal{W}^{r,\infty}(\mathcal{D})} = \max_{\boldsymbol{\nu} \in \mathbb{N}^p, |\boldsymbol{\nu}| \leq r} \text{ess sup}_{\mathbf{x} \in \mathcal{D}} |D^{\boldsymbol{\nu}} f(\mathbf{x})|,$$

where $\mathbb{N} = \{0, 1, 2, \dots\}$, $|\boldsymbol{\nu}| = \nu_1 + \dots + \nu_p$ for $\boldsymbol{\nu} = (\nu_1, \dots, \nu_p)^{\top} \in \mathbb{N}^p$, and $D^{\boldsymbol{\nu}} f(\mathbf{x}) = \frac{\partial^{|\boldsymbol{\nu}|} f(\mathbf{x})}{\partial x_1^{\nu_1} \dots \partial x_p^{\nu_p}}$. The space $\mathcal{W}^{r,\infty}(\mathcal{D})$ can be equivalently described as consisting of functions in $C^{r-1}(\mathcal{D})$ such that all their derivatives of order $(r-1)$ are Lipschitz continuous. For any $K > 0$, let $\mathcal{W}^{r,\infty}(\mathcal{D}, K)$ denote the ball centering at 0 of radius K in $\mathcal{W}^{r,\infty}(\mathcal{D})$, i.e.,

$$\mathcal{W}^{r,\infty}(\mathcal{D}, K) = \{f \in \mathcal{W}^{r,\infty}(\mathcal{D}) : \|f\|_{\mathcal{W}^{r,\infty}(\mathcal{D})} \leq K\}. \quad (11)$$

In Theorem 1, we establish a universal approximation theorem for the conditional Fréchet mean $m_{\oplus}(\cdot)$ under Assumptions 1–6 described as follows.

Assumption 1. For any $\mathbf{x} \in \mathbb{R}^p$ and $\boldsymbol{\theta}_L \in \Theta_L$, the minimizers $m_{\oplus}^{\text{NN}}(\mathbf{x}; \boldsymbol{\theta}_L)$ and $\hat{m}_{\oplus}^{\text{NN}}(\mathbf{x}; \boldsymbol{\theta}_L)$ defined in Eqs. (2) and (8), exist.

Assumption 2. Σ_{θ_L} is positive definite for any $\theta_L \in \Theta_L$, where Σ_{θ_L} is defined right after Eq. (3).

Assumption 3. There exists an integer $r_M \geq 1$ and a constant $K_M > 0$ such that $M(\omega, \cdot) \in \mathcal{W}^{r_M, \infty}(\mathcal{D}, K_M)$ for all $\omega \in \Omega$.

Assumption 4. There exists $\rho_\star > 0$ such that for any $\rho \in (0, \rho_\star]$,

$$\Delta(\rho) = \inf_{\mathbf{x} \in \mathcal{D}} \inf_{d\{\omega, m_{\oplus}(\mathbf{x})\} \geq \rho} \{M(\omega, \mathbf{x}) - M(m_{\oplus}(\mathbf{x}), \mathbf{x})\} > 0.$$

Assumption 5. There exists a constant $\lambda_\star > 0$ such that for any $L \geq 1$ and $\theta_L \in \Theta_L$, $\lambda_{\min}(\Sigma_{\theta_L}) \geq \lambda_\star$, where $\lambda_{\min}(\Sigma_{\theta_L})$ denotes the smallest eigenvalue of the matrix Σ_{θ_L} .

Assumption 6. There exist constants $W^\star, B^\star > 0$ such that θ_L satisfies $\prod_{l=1}^L \|\mathbf{W}_l\|_{\text{op}} \leq W^\star$ and $\sup_{1 \leq l \leq L} \|\mathbf{b}_l\| \leq B^\star$ for any integer $L \geq 1$.

Assumption 1 guarantees that the DFNN output, a global Fréchet regression evaluated at the final hidden layer representation, is well defined for every predictor input and parameter choice. Assumption 2 guarantees that the final layer covariance Σ_{θ_L} is nondegenerate, so $\Sigma_{\theta_L}^{-1}$ exists and the weight $s\{g_L(\mathbf{x}; \theta_L), g_L(\mathbf{X}; \theta_L)\}$ in Eq. (3) is well defined for each $\mathbf{x} \in \mathbb{R}^p$ almost surely. Assumption 3 requiring $M(\omega, \cdot) \in \mathcal{W}^{r_M, \infty}(\mathcal{D}, K_M)$ encodes that $M(\omega, \cdot)$ varies smoothly with the predictors for any $\omega \in \Omega$. This enables approximation rates by controlling how complex the target surface is over \mathcal{D} ; and it allows us to tie the depth and the width of the DFNN to the desired accuracy. In Assumption 4, $\Delta(\rho) > 0$ means that moving a distance ρ from $m_{\oplus}(\mathbf{x})$ raises the objective $M(m_{\oplus}(\mathbf{x}), \mathbf{x})$ uniformly in $\mathbf{x} \in \mathbb{R}^p$. This margin eliminates flat basins near the minimum and lets small objective errors imply small deviations away from the conditional Fréchet mean. Assumptions 1–4 imply the existence of a DFNN such that the corresponding predictions are arbitrarily close to the conditional Fréchet mean at an independent test point with arbitrarily high probability.

Additionally, under Assumptions 5 and 6, we show that there exists a DFNN such that the predictions are arbitrarily close to the conditional Fréchet mean uniformly over all inputs $\mathbf{x} \in \mathbb{R}^p$. Assumption 5 imposes a uniform lower bound $\lambda_{\min}(\Sigma_{\theta_L}) \geq \lambda_\star > 0$ for all $\theta_L \in \Theta_L$, strengthening Assumption 2 from pointwise positive definiteness to a global lower bound over the approximation class. Assumption 6 places norm constraints (Neyshabur et al., 2015; Bartlett et al., 2017) on $\prod_{l=1}^L \|\mathbf{W}_l\|_{\text{op}}$ and $\max_{1 \leq l \leq L} \|\mathbf{b}_l\|$, which uniformly control the magnitude of the final-layer representations which depends only on the depth L and input dimension p , but not on the particular weights—a key requirement for our approximation theorem.

Theorem 1. (i) Under Assumptions 1–6, for any $\varepsilon > 0$, there exists $\delta = \delta_\varepsilon > 0$, L_δ and $\theta_{L_\delta, \delta}$ such that $\sup_{\mathbf{x} \in \mathcal{D}} d\{m_{\oplus}^{\text{NN}}(\mathbf{x}; \theta_{L_\delta, \delta}), m_{\oplus}(\mathbf{x})\} < \varepsilon$.

(ii) Under Assumptions 1–4, for any $\varepsilon > 0$ and $\varepsilon' > 0$, there exists $\delta = \delta_{\varepsilon, \varepsilon'} > 0$, L_δ and $\theta_{L_\delta, \delta}$ such that $\mathbb{P}(d\{m_{\oplus}^{\text{NN}}(\mathbf{X}; \theta_{L_\delta, \delta}), m_{\oplus}(\mathbf{X})\} \geq \varepsilon) < \varepsilon'$.

The universal approximation theorem justifies DFNNs in practice; the next section demonstrates the practical performance of DFNNs through experiments on synthetic data and a real-world application.

4 Experiments

4.1 Implementation Details

We implement all deep neural networks in PyTorch with default parameter initializations for linear layers. Training uses stochastic gradient descent (SGD) with a fixed momentum of 0.9. For each experiment, we select the architectural and regularization-related hyperparameters—the number of hidden layers L , the width of hidden layers $\{p_l\}_{l=1}^L$, which are taken as the same value across first $L-1$ hidden layers, i.e., $p_l = p_1$ for all $l = 1, \dots, L-1$, the learning rate (LR), and the dropout rate (DR)—via a grid search, and then use the corresponding choices for that experiment. Grids of candidate values and the selected values are listed in Section A.1 in the Appendix.

To mitigate overfitting for the proposed DFNN, we implement a validation-based early stopping rule. The original training data is randomly split into a training set and a validation set in a 4-to-1 proportion. The DFNN is trained only on the training set. After a fixed burn-in period of N_{initial} epochs, we evaluate the validation loss—given by the mean squared prediction error (MSPE) on the validation set—for each epoch, and stop training if the validation loss at the current epoch fails to improve by at least $\delta_{\text{tolerance}}$ compared with the previous epoch over N_{patience} consecutive epochs. Then we use the weights with which the DFNN achieves the lowest validation loss observed before stopping. The selection of the hyperparameters in the early stopping rule, i.e., N_{initial} , $\delta_{\text{tolerance}}$, and N_{patience} , are detailed in Section A.2 in the Appendix for each scenario in the experiments.

4.2 Experiment Setups

To evaluate the effectiveness of our proposed DFNN framework, we perform empirical experiments on both synthetic data and real-world data. Our experiments cover responses lying in three different types of metric spaces. First, we consider the Wasserstein space of univariate probability measures endowed with the 2-Wasserstein metric (Villani, 2008). We simulate data with responses in the Wasserstein space in Experiment 1 below. Second, we consider the space of graph Laplacian matrices with the Frobenius metric and simulate data with network-valued responses in this space in Experiment 2 below. Third, we handle compositional responses in Experiment 3, which are viewed as random objects lying in the 8-simplex $\Delta^8 = \{\mathbf{a} \in [0, 1]^9 : \sum_{j=1}^9 a_j = 1\}$, endowed with the Aitchison distance given by the Euclidean metric between the centered log-ratios of compositions (Aitchison, 1986).

In each experiment with simulated data (Experiments 1–2), we compare the proposed DFNN with other methods, including: global Fréchet regression (GFR) (Petersen and Müller, 2019), local Fréchet regression with sufficient dimension reduction (SDR) (Zhang et al., 2024), and deep Fréchet regression (DFR) (Iao et al., 2025). For DFR, we follow the selection of hyperparameters for the architecture and regularization in Iao et al. (2025), see Table 12 in Section B.1 in the Appendix. For our DFNN, we choose the hyperparameters for the architecture and regularization following the procedures in Section 4.1, and the grids of candidate values and chosen values are listed in Section A.1 in the Appendix. For the real-data application (Experiment 3), as Iao et al. (2025) did not implement DFR for compositional responses, we compare our DFNN with standard DNNs (referred to as DNN in the following) instead of DFR, as well as GFR and SDR. For DNN, we treat compositional responses as

Euclidean responses and use the same choices of the architectural and regularization-related hyperparameters as DFNN.

We evaluate the performance of each method by the mean squared prediction error (MSPE). For each experiment with simulated data (Experiments 1–2), for each Monte Carlo run out of $B = 250$ runs, we generate a training sample of size n , $\{(\mathbf{X}_i, Y_i)\}_{i=1}^n$, and a test set of 100 additional pairs $\{(\mathbf{X}_{n+i}, Y_{n+i})\}_{i=1}^{100}$, and evaluate the MSPE on the test set, which is defined as

$$\text{MSPE} = \frac{1}{100} \sum_{i=1}^{100} d^2(\hat{Y}_{n+i}, Y_{n+i}), \quad (12)$$

where \hat{Y}_{n+i} is the prediction of Y_{n+i} given by the corresponding method, e.g., for the proposed DFNN, $\hat{Y}_{n+i} = \hat{Y}(\mathbf{X}_{n+i})$ with $\hat{Y}(\cdot)$ defined in Eq. (10). For the experiment with real-world data (Experiment 3), we perform 10-fold cross-validation. The sample is randomly split into 10 folds, and each fold is left out as a test set, respectively. The prediction of a response Y_i that belongs to the k th fold for some $k = 1, \dots, 10$ is given by the model trained on the other 9 folds except for the k th fold, denoted by $\hat{Y}_{i,\text{cv}}$, for $i = 1, \dots, n$. For DNN, of which the output predictions may not lie within the simplex, the predictions are first projected back to the simplex before calculating the MSPE. The MSPE is defined as

$$\text{MSPE} = \frac{1}{n} \sum_{i=1}^n d^2(\hat{Y}_{i,\text{cv}}, Y_i), \quad (13)$$

If there exist zero entries in the predicted compositions, they are replaced by 10^{-8} before computing the Aitchison metric, which is ill-defined in the existence of zero entries. We repeat the random splits 100 times and each time evaluate the MSPE as defined in Eq. (13).

In the following, we describe the data in each experiment.

Experiment 1. (Simulated data with distributional responses.) Here we investigate performance of predicting distributional responses. In each Monte Carlo run, a training sample of n i.i.d. pairs, $\{(\mathbf{X}_i, Y_i)\}_{i=1}^n$, are generated as follows. For each $i = 1, \dots, n$, we generate the predictors $\mathbf{X}_i = (X_{i,1} \dots, X_{i,10})^\top$ such that $(X_{i,1}, \dots, X_{i,4})^\top, X_{i,5}, \dots, X_{i,10}$ are mutually independent and that

$$(X_{i,1}, \dots, X_{i,4})^\top \sim \mathcal{N}(\mathbf{0}, \Sigma_{0.1}), \quad \Sigma_\rho = \begin{pmatrix} 1 & \rho & \cdots & \rho \\ \rho & 1 & \cdots & \rho \\ \vdots & \vdots & \ddots & \vdots \\ \rho & \rho & \cdots & 1 \end{pmatrix} \in \mathbb{R}^{4 \times 4},$$

$$X_{i,j} \sim \mathcal{N}(1, 1), \quad j \in \{5, 6, 7, 8, 9\},$$

$$X_{i,j} \sim \text{Bernoulli}(0.3), \quad j \in \{10\}.$$

For each $i = 1, \dots, n$, define

$$\mu_i = X_{i,1} \cos(\pi X_{i,2}) - 0.5 X_{i,3}^2 + 4 \log(1 + X_{i,4}^2) - 4(1 + |X_{i,5}|)^{-1},$$

$$\theta_i = 0.5 + 3.5 \text{expit}\{2X_{i,6}X_{i,10} + 2X_{i,9}^2 \sin(\pi X_{i,8}) + 4(1 + X_{i,7})^{-1}\},$$

where $\text{expit}(t) = 1/(1+e^{-t})$ for $t \in \mathbb{R}$. For each $i = 1, \dots, n$, conditioning on \mathbf{X}_i , we generate η_i and σ_i as

$$\eta_i \mid \mathbf{X}_i \sim \mathcal{N}(\mu_i, 0.5^2) \quad \text{and} \quad \sigma_i \mid \mathbf{X}_i \sim \text{Gamma}(\theta_i^2, \theta_i^{-1})$$

and define $Y_i = \mathcal{N}(\eta_i, \sigma_i^2)$. Furthermore, for each $i = 1, \dots, n$, we draw a random sample of independent data points $\{Z_{i,k}\}_{k=1}^{100}$ from Y_i , and use the empirical quantile function of $\{Z_{i,k}\}_{k=1}^{100}$ as the surrogate of Y_i in the training data. We perform the experiment with training samples of size $n \in \{200, 500, 1000\}$, respectively.

Experiment 2. (Simulated data with network-valued responses represented by graph Laplacian matrices.) We consider responses being graph Laplacian matrices of networks with q nodes. For each Monte Carlo run, we first generate a binary mask matrix $\mathbf{A} \in \{0, 1\}^{q \times q}$ encoding the presence of edges, with $A_{k,\ell} = A_{\ell,k} \sim \text{Bernoulli}(0.3)$ for any $k, \ell \in \{1, 2, \dots, q\}$ with $k < \ell$ independently, and $A_{k,k} = 0$ for all $k \in \{1, 2, \dots, q\}$. For each $i = 1, \dots, n$, we generate $X_{i,1}, \dots, X_{i,10}$ i.i.d. from $\text{Unif}(0, 1)$, and define $\mathbf{X}_i = (X_{i,1}, \dots, X_{i,10})^\top$. Conditioning on \mathbf{X}_i and \mathbf{A} , we generate a symmetric edge-weight matrix $\mathbf{E}_i = (E_{i,k,\ell})_{1 \leq k, \ell \leq q}$ on the connected edges as:

$$E_{i,k,\ell} = \begin{cases} \sin\left(\frac{(k+\ell)\pi}{2q}\right) \cdot \frac{1}{|X_{ik}|+1} \cdot (2 + X_{i\ell}^2) + \varepsilon_{i,k,\ell} & \text{if } k < \ell \text{ and } A_{k,\ell} \neq 0 \\ E_{i,\ell,k} & \text{if } k > \ell \\ 0 & \text{if } k = \ell \end{cases}$$

where $\varepsilon_{i,k,\ell} \sim \text{Unif}(-a, a)$ are additional noises generated independently across (i, k, ℓ) with $a = 0$ corresponding to noiseless scenarios and larger values of a corresponding to higher levels of noise. Let \mathbf{D}_i be the degree matrix of \mathbf{E}_i , i.e., a diagonal matrix with diagonal elements given by $\mathbf{E}_i \mathbf{1}_q$, where $\mathbf{1}_q$ denotes the q -dimensional vector with all entries equal to 1. Then we define $Y_i \in \mathbb{R}^{q \times q}$ as

$$Y_i = \mathbf{D}_i - \mathbf{E}_i.$$

We perform the experiment with training samples of size $n \in \{200, 500, 1000\}$, number of nodes $q = 10$, in different levels of noise with $a \in \{0, 0.02, 0.1\}$, respectively.

Experiment 3. (Real-world data with the compositional responses.) The state-level employment data from the Federal Reserve Economic Data (FRED) report employment counts in nine occupational subclasses: (1) Mining and Logging; (2) Construction; (3) Manufacturing; (4) Trade, Transportation, and Utilities; (5) Information; (6) Professional and Business Services; (7) Leisure and Hospitality; (8) Other Services; and (9) Government. We focus on the year 2010 and consider the 49 states except for Hawaii, which is excluded due to missing records. The responses are the employment occupational compositions for each state, represented as a 9-dimensional vector of occupational subclass shares summing to one. In addition, we assemble state-level economic, demographic, and geographic information from the Federal Reserve Economic Data (FRED), the U.S. Bureau of Labor Statistics (BLS), and the U.S. Census Bureau, which turns to be 17 predictors as listed in Table 1. See Section B.2 in the Appendix for more details about the data.

4.3 Results

For Experiment 1, MSPEs over $B = 250$ Monte Carlo runs for different methods are summarized in Table 2 and Figure 1. Notably, DFNN consistently outperforms all other methods in both average and standard deviation of MSPE across all considered sample sizes, demonstrating superior predictive performance in terms of both prediction accuracy and stability.

Table 1: State-level predictors used in the employment composition analysis.

Index	Variable	Explanation
1	Unemployment rate	percentage of unemployed individuals
2	Income	annual median household income
3	GDP	state-level gross domestic product
4	Minimum wage	state minimum hourly wage
5	RPP	relative housing cost index (national average = 100)
6	HPI	index of housing price trends based on transactions
7	Business	number of new business applications
8	Part-time rate	involuntary part-time employment rate
9	U-6 rate	a broader unemployment measure
10	Urbanization	share of population in urban areas
11	Population density	residents per square mile
12	Population	total number of residents
13	Sex ratio	male-to-female population ratio
14	Homeownership	share of owner-occupied housing units
15	Rental	rental vacancy rate
16	Education	proportion with a bachelor's degree or higher
17	Insurance coverage	uninsured population rate

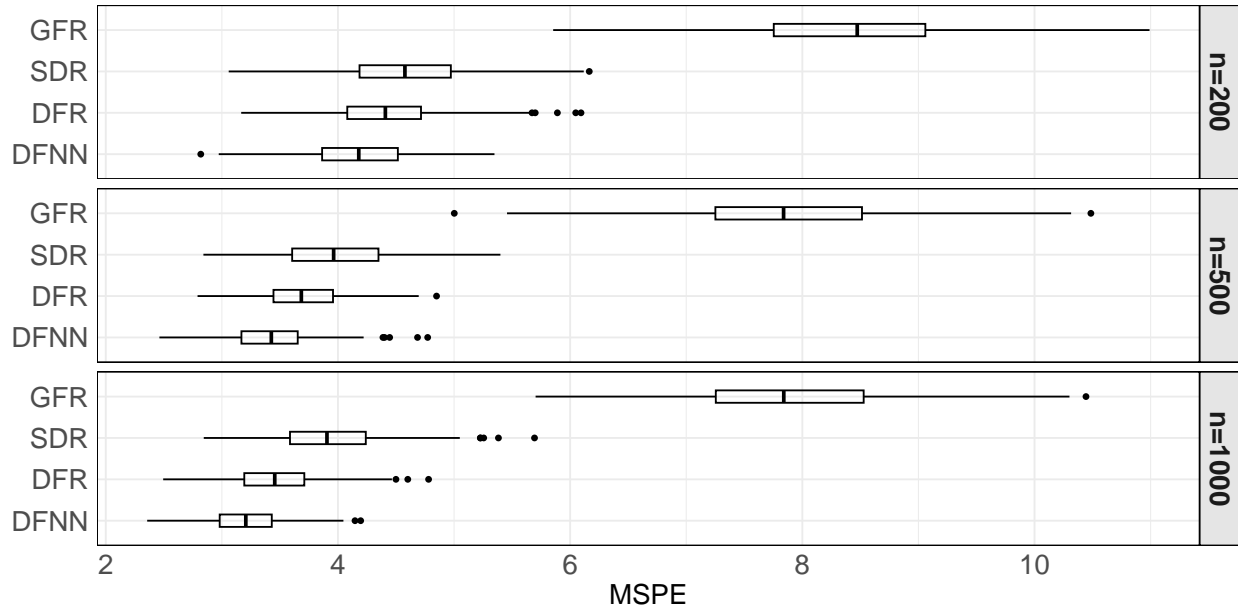


Figure 1: Boxplots of MSPEs for GFR, SDR, DFR, and DFNN for Experiment 1 with sample size $n \in \{200, 500, 1000\}$.

For Experiment 2, MSPEs over $B = 250$ Monte Carlo runs are summarized in Figure 2 and Tables 3–5. While MSPEs increase at higher levels of noise, DFNN attains the lowest average errors and smallest variances across all sample sizes and for noiseless data and data

Table 2: Average and standard deviation (in parentheses) of MSPEs of GFR, SDR, DFR, and DFNN for Experiment 1 with sample size $n \in \{200, 500, 1000\}$.

n	GFR	SDR	DFR	DFNN
200	8.42 (0.99)	4.63 (0.57)	4.43 (0.51)	4.20 (0.50)
500	7.84 (0.93)	3.99 (0.51)	3.71 (0.40)	3.44 (0.39)
1000	7.90 (0.93)	3.95 (0.50)	3.47 (0.40)	3.21 (0.34)

contaminated with different levels of noise.

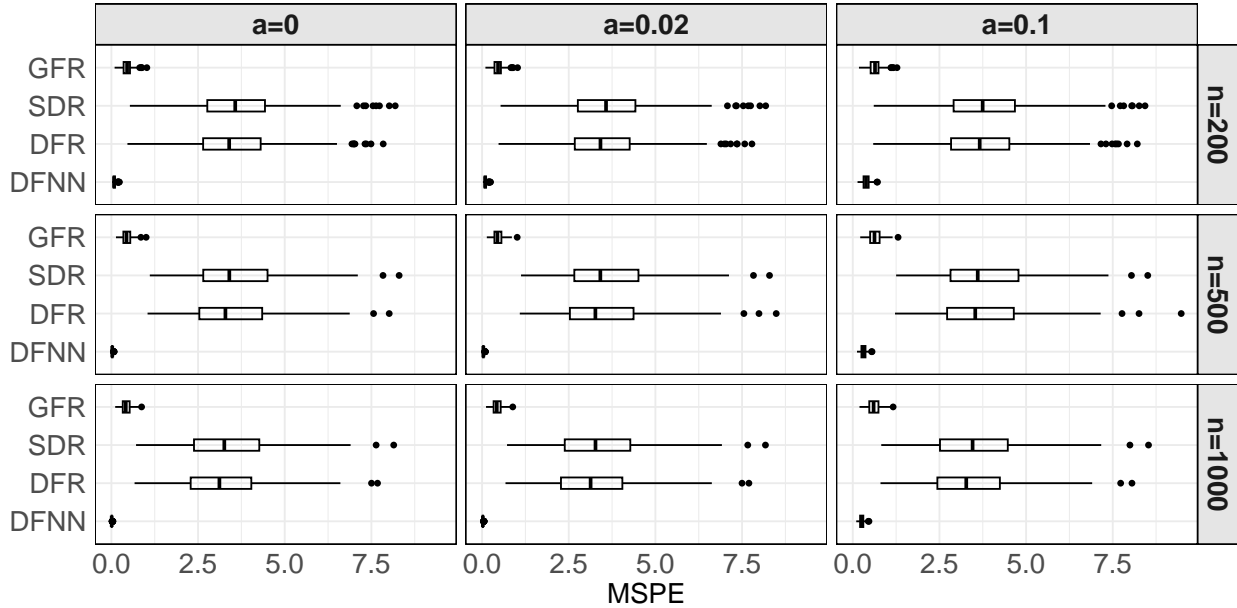


Figure 2: Boxplots of MSPEs for GFR, SDR, DFR, and DFNN for Experiment 2 with sample size $n \in \{200, 500, 1000\}$ and different levels of noise ($a = 0$ corresponding to noiseless settings and larger a corresponding to higher levels of noise). Three outliers with MSPE values above 10, all from the DFR method, occurred under the settings $(n = 200, a = 0.02)$, $(n = 1000, a = 0.02)$, and $(n = 1000, a = 0.1)$, and are omitted for visualization purposes.

Table 3: Average and standard deviation (in parentheses) of MSPEs of GFR, SDR, DFR, and DFNN for Experiment 2 in noiseless settings ($a = 0$) with sample size $n \in \{200, 500, 1000\}$.

n	GFR	SDR	DFR	DFNN
200	0.459 (0.151)	3.725 (1.419)	3.574 (1.367)	0.085 (0.033)
500	0.454 (0.144)	3.637 (1.308)	3.490 (1.274)	0.028 (0.013)
1000	0.427 (0.143)	3.351 (1.311)	3.193 (1.261)	0.011 (0.007)

For Experiment 3, MSPEs from 100 times 10-fold cross-validation are summarized in Figure 3 and Table 6. DFNN again outperforms all the other methods.

Table 4: Average and standard deviation (in parentheses) of MSPEs of GFR, SDR, DFR, and DFNN for Experiment 2 in settings of a lower level of noise ($a = 0.02$) with sample size $n \in \{200, 500, 1000\}$.

n	GFR	SDR	DFR	DFNN
200	0.466 (0.152)	3.734 (1.422)	3.617 (1.487)	0.096 (0.036)
500	0.461 (0.146)	3.645 (1.309)	3.502 (1.307)	0.040 (0.016)
1000	0.435 (0.145)	3.360 (1.315)	3.526 (5.236)	0.023 (0.009)

Table 5: Average and standard deviation (in parentheses) of MSPEs of GFR, SDR, DFR, and DFNN for Experiment 2 in settings of a higher level of noise ($a = 0.1$) with sample size $n \in \{200, 500, 1000\}$.

n	GFR	SDR	DFR	DFNN
200	0.649 (0.191)	3.928 (1.466)	3.798 (1.415)	0.384 (0.104)
500	0.643 (0.186)	3.831 (1.345)	3.733 (1.369)	0.312 (0.084)
1000	0.608 (0.185)	3.537 (1.357)	3.538 (2.714)	0.261 (0.069)

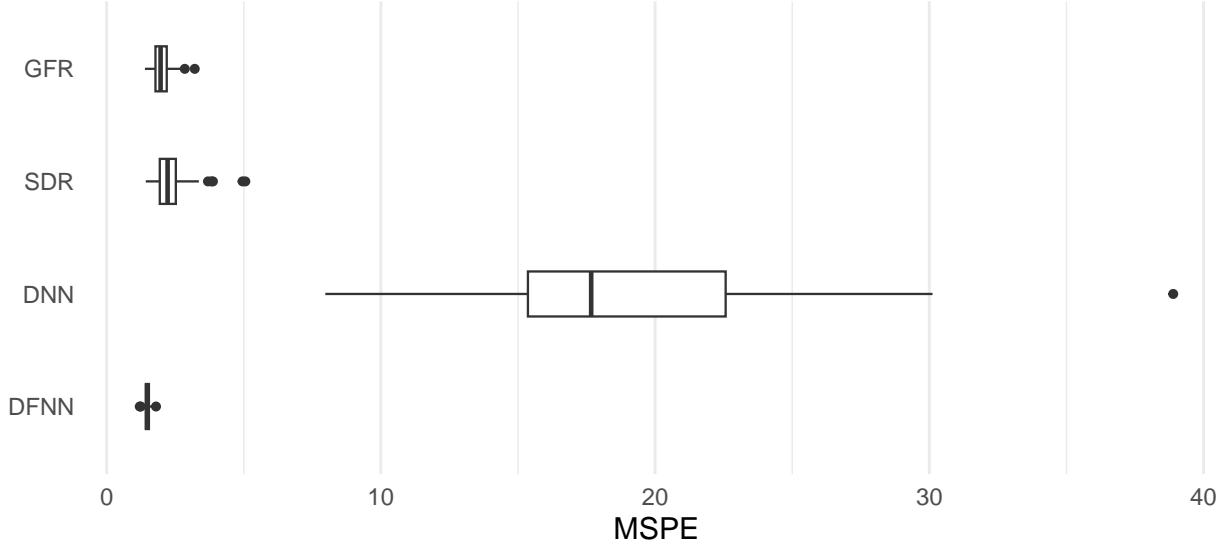


Figure 3: Boxplots of MSPEs from 100 times 10-fold cross-validation for GFR, SDR, DFR, and DFNN for Experiment 3.

5 Discussion

This work proposes DFNNs as an end-to-end framework for regression with responses in metric spaces, combining a weighted Fréchet mean output layer with standard hidden-layer representations and training via empirical Fréchet risk minimization. For the special case of Euclidean responses, the proposed DFNNs reduce to classical DNNs. We establish the

Table 6: Average and standard deviation (in parentheses) of MSPEs of GFR, SDR, DNN, and DFNN for Experiment 3.

GFR	SDR	DNN	DFNN
2.02 (0.32)	2.34 (0.61)	18.95 (5.78)	1.48 (0.11)

universal approximation result that, under mild regularity conditions, DFNNs can approximate the conditional Fréchet mean up to arbitrary accuracy. We also show in empirical experiments that DFNNs outperform state-of-the-art methods for regression with metric-space-valued responses. Future work includes principled metric selection and analyzing the algorithmic aspects of DFNN training.

References

Aguech, M. and G. Carlier (2011). Barycenters in the Wasserstein space. *SIAM Journal on Mathematical Analysis* 43(2), 904–924.

Ahidar-Coutrix, A., T. Le Gouic, and Q. Paris (2020). Convergence rates for empirical barycenters in metric spaces: Curvature, convexity and extendable geodesics. *Probability Theory and Related Fields* 177, 323–368.

Aissa, A. F., A. B. Islam, M. M. Ariss, C. C. Go, A. E. Rader, R. D. Conrardy, A. M. Gajda, C. Rubio-Perez, K. Valyi-Nagy, M. Pasquinelli, et al. (2021). Single-cell transcriptional changes associated with drug tolerance and response to combination therapies in cancer. *Nature Communications* 12(1), 1628.

Aitchison, J. (1982). The statistical analysis of compositional data (with discussion). *Journal of the Royal Statistical Society: Series B* 44(2), 139–177.

Aitchison, J. (1986). *The Statistical Analysis of Compositional Data*. Chapman & Hall, Ltd.

Bartlett, P. L., D. J. Foster, and M. J. Telgarsky (2017). Spectrally-normalized margin bounds for neural networks. *Advances in Neural Information Processing Systems* 30, 6240–6249.

Bellet, A., A. Habrard, and M. Sebban (2015). *Metric Learning*. Morgan & Claypool Publishers.

Bennett, I. J., D. J. Madden, C. J. Vaidya, D. V. Howard, and J. H. Howard Jr (2010). Age-related differences in multiple measures of white matter integrity: A diffusion tensor imaging study of healthy aging. *Human Brain Mapping* 31(3), 378–390.

Bhattacharjee, S., B. Li, and L. Xue (2025). Nonlinear global Fréchet regression for random objects via weak conditional expectation. *The Annals of Statistics* 53(1), 117–143.

Bhattacharjee, S. and H.-G. Müller (2023). Single index Fréchet regression. *The Annals of Statistics* 51(4), 1770–1798.

Bhattacharya, R. and V. Patrangenaru (2002, November). Nonparametric estimation of location and dispersion on Riemannian manifolds. *Journal of Statistical Planning and Inference* 108(1–2), 23–35.

Bigot, J., R. Gouet, T. Klein, and A. López (2017). Geodesic PCA in the Wasserstein space by convex PCA. *Annales de l’Institut Henri Poincaré, Probabilités et Statistiques* 53(1),

1–26.

Bronstein, M. M., J. Bruna, Y. LeCun, A. Szlam, and P. Vandergheynst (2017). Geometric deep learning: Going beyond Euclidean data. *IEEE Signal Processing Magazine* 34(4), 18–42.

Brooks, D., O. Schwander, F. Barbaresco, J.-Y. Schneider, and M. Cord (2019). Riemannian batch normalization for SPD neural networks. *Advances in Neural Information Processing Systems* 32, 15489–15500.

Brunel, V.-E. and J. Serres (2024). Concentration of empirical barycenters in metric spaces. In *International Conference on Algorithmic Learning Theory*, pp. 337–361. PMLR.

Calissano, A., A. Feragen, and S. Vantini (2022). Graph-valued regression: Prediction of unlabelled networks in a non-Euclidean graph space. *Journal of Multivariate Analysis* 190, 104950.

Capitaine, L., J. Bigot, R. Thiébaut, and R. Genuer (2024). Fréchet random forests for metric space valued regression with non Euclidean predictors. *Journal of Machine Learning Research* 25(355), 1–41.

Cazelles, E., V. Seguy, J. Bigot, M. Cuturi, and N. Papadakis (2018). Geodesic PCA versus log-PCA of histograms in the Wasserstein space. *SIAM Journal on Scientific Computing* 40(2), B429–B456.

Chakraborty, R., J. Bouza, J. H. Manton, and B. C. Vemuri (2020). ManifoldNet: A deep neural network for manifold-valued data with applications. *IEEE Transactions on Pattern Analysis and Machine Intelligence* 44(2), 799–810.

Chami, I., Z. Ying, C. Ré, and J. Leskovec (2019). Hyperbolic graph convolutional neural networks. *Advances in Neural Information Processing Systems* 32, 4868–4879.

Chang, T. (1989). Spherical regression with errors in variables. *The Annals of Statistics* 17, 293–306.

Chen, H. and H.-G. Müller (2023). Sliced Wasserstein regression. *arXiv preprint arXiv:2306.10601*.

Chen, W., X. Han, Y. Lin, H. Zhao, Z. Liu, P. Li, M. Sun, and J. Zhou (2022, May). Fully hyperbolic neural networks. In S. Muresan, P. Nakov, and A. Villavicencio (Eds.), *Proceedings of the 60th Annual Meeting of the Association for Computational Linguistics (Volume 1: Long Papers)*, Dublin, Ireland, pp. 5672–5686. Association for Computational Linguistics.

Chen, Y., Z. Lin, and H.-G. Müller (2023). Wasserstein regression. *Journal of the American Statistical Association* 118(542), 869–882.

Chen, Y. and H.-G. Müller (2022). Uniform convergence of local Fréchet regression with applications to locating extrema and time warping for metric space valued trajectories. *The Annals of Statistics* 50(3), 1573–1592.

Chen, Z., T. Xu, X.-J. Wu, R. Wang, Z. Huang, and J. Kittler (2023). Riemannian local mechanism for SPD neural networks. In *Proceedings of the AAAI Conference on Artificial Intelligence*, Volume 37, pp. 7104–7112.

Choi, C., Z. Lin, and B. U. Park (2025). High-dimensional partially linear additive models on Riemannian manifolds. *Bernoulli* 31(4), 3285–3308.

Cohen, T. S., M. Geiger, J. Köhler, and M. Welling (2018). Spherical CNNs. In *International Conference on Learning Representations*.

Coors, B., A. P. Condurache, and A. Geiger (2018, September). SphereNet: Learning spher-

ical representations for detection and classification in omnidirectional images. In *Proceedings of the European Conference on Computer Vision (ECCV)*, pp. 518–533.

Cornea, E., H. Zhu, P. Kim, and J. G. Ibrahim (2017). Regression models on Riemannian symmetric spaces. *Journal of the Royal Statistical Society: Series B* 79(2), 463–482.

Davis, B. C., P. T. Fletcher, E. Bullitt, and S. Joshi (2007). Population shape regression from random design data. In *2007 IEEE 11th International Conference on Computer Vision*.

Di Marzio, M., A. Panzera, and C. C. Taylor (2014). Nonparametric regression for spherical data. *Journal of the American Statistical Association* 109(506), 748–763.

Dong, Y. and Y. Wu (2022). Fréchet kernel sliced inverse regression. *Journal of Multivariate Analysis* 191, 105032.

Dryden, I. L. and K. V. Mardia (2016). *Statistical Shape Analysis: With Applications in R*, Volume 995. John Wiley & Sons.

Dubey, P., Y. Chen, and H.-G. Müller (2024). Metric statistics: Exploration and inference for random objects with distance profiles. *The Annals of Statistics* 52(2), 757–792.

Fair, D. A., A. L. Cohen, N. U. Dosenbach, J. A. Church, F. M. Miezin, D. M. Barch, M. E. Raichle, S. E. Petersen, and B. L. Schlaggar (2008). The maturing architecture of the brain’s default network. *Proceedings of the National Academy of Sciences* 105(10), 4028–4032.

Fan, J. and H.-G. Müller (2024). Conditional Wasserstein barycenters and interpolation/extrapolation of distributions. *IEEE Transactions on Information Theory* 71(5), 3835–3853.

Fang, Z., H. Feng, S. Huang, and D.-X. Zhou (2020). Theory of deep convolutional neural networks II: Spherical analysis. *Neural Networks* 131, 154–162.

Faraway, J. J. (2014). Regression for non-Euclidean data using distance matrices. *Journal of Applied Statistics* 41, 2342–2357.

Filzmoser, P., K. Hron, and M. Templ (2018). *Applied Compositional Data Analysis: With Worked Examples in R*. Springer.

Fisher, N. I. (1995). *Statistical analysis of circular data*. Cambridge University Press.

Fisher, N. I., T. Lewis, and B. J. J. Embleton (1987). *Statistical Analysis of Spherical Data*. Cambridge: Cambridge University Press.

Fréchet, M. (1948). Les éléments aléatoires de nature quelconque dans un espace distancié. In *Annales de l’Institut Henri Poincaré*, Volume 10, pp. 215–310.

Ganea, O., G. Béćigneul, and T. Hofmann (2018). Hyperbolic neural networks. *Advances in Neural Information Processing Systems* 31, 5345–5355.

Ghodrati, L. and V. M. Panaretos (2022). Distribution-on-distribution regression via optimal transport maps. *Biometrika* 109(4), 957–974.

Ghodrati, L. and V. M. Panaretos (2023). Transportation of measure regression in higher dimensions. *arXiv preprint arXiv:2305.17503*.

Ghojogh, B., M. Crowley, F. Karray, and A. Ghodsi (2023). *Elements of Dimensionality Reduction and Manifold Learning*. Springer.

Ghosal, A., W. Meiring, and A. Petersen (2023). Fréchet single index models for object response regression. *Electronic Journal of Statistics* 17(1), 1074–1112.

Greenacre, M. (2021). Compositional data analysis. *Annual Review of Statistics and its Application* 8(1), 271–299.

Greenacre, M., E. Grunsky, J. Bacon-Shone, I. Erb, and T. Quinn (2023). Aitchison’s

compositional data analysis 40 years on: A reappraisal. *Statistical Science* 38(3), 386–410.

Guégan, D. and M. Iacopini (2018). Nonparametric forecasting of multivariate probability density functions. *arXiv preprint arXiv:1803.06823*.

Gulcehre, C., M. Denil, M. Malinowski, A. Razavi, R. Pascanu, K. M. Hermann, P. Battaglia, V. Bapst, D. Raposo, A. Santoro, and N. de Freitas (2019). Hyperbolic attention networks. In *International Conference on Learning Representations*.

Han, K., H.-G. Müller, and B. U. Park (2020). Additive functional regression for densities as responses. *Journal of the American Statistical Association* 115(530), 997–1010.

Hein, M. (2009). Robust nonparametric regression with metric-space valued output. In *Advances in Neural Information Processing Systems*, pp. 718–726.

Hinkle, J., P. Muralidharan, P. T. Fletcher, and S. Joshi (2012). Polynomial regression on Riemannian manifolds. In A. Fitzgibbon, S. Lazebnik, P. Perona, Y. Sato, and C. Schmid (Eds.), *Computer Vision–ECCV 2012*, pp. 1–14. Berlin: Springer.

Hron, K., J. Machalová, and A. Menafooglio (2023). Bivariate densities in Bayes spaces: Orthogonal decomposition and spline representation. *Statistical Papers* 64(5), 1629–1667.

Hron, K., A. Menafooglio, M. Templ, K. Hrúzová, and P. Filzmoser (2016). Simplicial principal component analysis for density functions in Bayes spaces. *Computational Statistics and Data Analysis* 94, 330–350.

Huang, Z. and L. Van Gool (2017). A Riemannian network for SPD matrix learning. In *Proceedings of the AAAI conference on artificial intelligence*, Volume 31, pp. 2036–2042.

Huckemann, S. and B. Eltzner (2021). Data analysis on nonstandard spaces. *Wiley Interdisciplinary Reviews: Computational Statistics* 13(3), e1526.

Iao, S. I., Y. Zhou, and H.-G. Müller (2025). Deep Fréchet regression. *Journal of the American Statistical Association*, to appear.

Jäntti, M. and S. P. Jenkins (2010). The impact of macroeconomic conditions on income inequality. *Journal of Economic Inequality* 8(2), 221–240.

Jupp, P. E. and J. T. Kent (1987). Fitting smooth paths to spherical data. *Journal of the Royal Statistical Society Series C: Applied Statistics* 36(1), 34–46.

Kim, Y.-H. and B. Pass (2017). Wasserstein barycenters over Riemannian manifolds. *Advances in Mathematics* 307, 640–683.

Kipf, T. N. and M. Welling (2017). Semi-supervised classification with graph convolutional networks. In *International Conference on Learning Representations*.

Kurisu, D. and T. Otsu (2025). Model averaging for global Fréchet regression. *Journal of Multivariate Analysis* 207, 105416.

Le Gouic, T. and J.-M. Loubes (2017). Existence and consistency of Wasserstein barycenters. *Probability Theory and Related Fields* 168(3-4), 901–917.

Le Gouic, T., Q. Paris, P. Rigollet, and A. J. Stromme (2022). Fast convergence of empirical barycenters in Alexandrov spaces and the Wasserstein space. *Journal of the European Mathematical Society*. (in press).

Li, B., C. Yoon, and J. Ahn (2023). Reproducing kernels and new approaches in compositional data analysis. *Journal of Machine Learning Research* 24(327), 1–34.

Lin, L., B. St. Thomas, H. Zhu, and D. B. Dunson (2017). Extrinsic local regression on manifold-valued data. *Journal of the American Statistical Association* 112(519), 1261–1273.

Lin, Z. and H.-G. Müller (2021). Total variation regularized Fréchet regression for metric-space valued data. *The Annals of Statistics* 49(6), 3510–3533.

Lin, Z., H.-G. Müller, and B. U. Park (2023). Additive models for symmetric positive-definite matrices and lie groups. *Biometrika* 110(2), 361–379.

Liu, Q., M. Nickel, and D. Kiela (2019). Hyperbolic graph neural networks. *Advances in Neural Information Processing Systems* 32, 8230–8241.

Maier, E.-M., A. Stöcker, B. Fitzenberger, and S. Greven (2025). Additive density-on-scalar regression in Bayes Hilbert spaces with an application to gender economics. *The Annals of Applied Statistics* 19(1), 680–700.

Mardia, K. V. and P. E. Jupp (2009). *Directional Statistics*. Hoboken: John Wiley & Sons.

Marron, J. S. and A. M. Alonso (2014). Overview of object oriented data analysis. *Biometrical Journal* 56(5), 732–753.

Marron, J. S. and I. L. Dryden (2021). *Object Oriented Data Analysis*. CRC Press.

Masci, J., D. Boscaini, M. Bronstein, and P. Vandergheynst (2015). Geodesic convolutional neural networks on Riemannian manifolds. In *Proceedings of the IEEE International Conference on Computer Vision Workshops*, pp. 37–45.

Müller, H.-G. (2016). Peter Hall, functional data analysis and random objects. *The Annals of Statistics* 44(5), 1867–1887.

Neyshabur, B., R. Tomioka, and N. Srebro (2015, 03–06 Jul). Norm-based capacity control in neural networks. In P. Grünwald, E. Hazan, and S. Kale (Eds.), *Proceedings of The 28th Conference on Learning Theory*, Volume 40 of *Proceedings of Machine Learning Research*, Paris, France, pp. 1376–1401. PMLR.

Nguyen, X. S. (2021). GeomNet: A neural network based on Riemannian geometries of SPD matrix space and Cholesky space for 3D skeleton-based interaction recognition. In *Proceedings of the IEEE/CVF International Conference on Computer Vision*, pp. 13379–13389.

Nguyen, X. S., L. Brun, O. Lézoray, and S. Bougleux (2019). A neural network based on SPD manifold learning for skeleton-based hand gesture recognition. In *Proceedings of the IEEE/CVF Conference on Computer Vision and Pattern Recognition*, pp. 12036–12045.

Nickel, M. and D. Kiela (2017). Poincaré embeddings for learning hierarchical representations. *Advances in Neural Information Processing Systems* 30, 6338–6347.

Ohta, S.-I. (2012). Barycenters in Alexandrov spaces of curvature bounded below. *Advances in Geometry* 12(4), 571–587.

Okano, R. and M. Imaizumi (2023). Distribution-on-distribution regression with Wasserstein metric: Multivariate Gaussian case. *arXiv preprint arXiv:2307.06137*.

Oliva, J., B. Póczos, and J. Schneider (2013). Distribution to distribution regression. In *International Conference on Machine Learning*, pp. 1049–1057.

Pan, Y.-T., J.-L. Chou, and C.-S. Wei (2022). MAtt: A manifold attention network for EEG decoding. *Advances in Neural Information Processing Systems* 35, 31116–31129.

Pegoraro, M. and M. Beraha (2022). Projected statistical methods for distributional data on the real line with the Wasserstein metric. *Journal of Machine Learning Research* 23(1), 1686–1744.

Peng, W., T. Varanka, A. Mostafa, H. Shi, and G. Zhao (2021). Hyperbolic deep neural networks: A survey. *IEEE Transactions on Pattern Analysis and Machine Intelligence* 44(12), 10023–10044.

Petersen, A., C.-J. Chen, and H.-G. Müller (2019). Quantifying and visualizing intraregional connectivity in resting-state functional magnetic resonance imaging with correlation densities. *Brain Connectivity* 9(1), 37–47.

Petersen, A., S. Deoni, and H.-G. Müller (2019). Fréchet estimation of time-varying covariance matrices from sparse data, with application to the regional co-evolution of myelination in the developing brain. *The Annals of Applied Statistics* 13(1), 393–419.

Petersen, A. and H.-G. Müller (2016). Functional data analysis for density functions by transformation to a Hilbert space. *The Annals of Statistics* 44(1), 183–218.

Petersen, A. and H.-G. Müller (2019). Fréchet regression for random objects with Euclidean predictors. *The Annals of Statistics* 47(2), 691–719.

Petersen, A., C. Zhang, and P. Kokoszka (2022). Modeling probability density functions as data objects. *Econometrics and Statistics* 21, 159–178.

Prentice, M. J. (1989). Spherical regression on matched pairs of orientation statistics. *Journal of the Royal Statistical Society: Series B*, 241–248.

Qiu, R., Z. Yu, and R. Zhu (2024). Random forest weighted local Fréchet regression with random objects. *Journal of Machine Learning Research* 25(107), 1–69.

Scealy, J. L. and A. H. Welsh (2011). Regression for compositional data by using distributions defined on the hypersphere. *Journal of the Royal Statistical Society: Series B (Statistical Methodology)* 73(3), 351–375.

Scealy, J. L. and A. H. Welsh (2017). A directional mixed effects model for compositional expenditure data. *Journal of the American Statistical Association* 112(517), 24–36.

Scealy, J. L. and A. T. Wood (2019). Scaled von Mises–Fisher distributions and regression models for paleomagnetic directional data. *Journal of the American Statistical Association* 114(528), 1547–1560.

Schötz, C. (2019). Convergence rates for the generalized Fréchet mean via the quadruple inequality. *Electronic Journal of Statistics* 13(2), 4280–4345.

Schötz, C. (2020). Regression in nonstandard spaces with Fréchet and geodesic approaches. *arXiv preprint arXiv:2012.13332*.

Schötz, C. (2022). Nonparametric regression in nonstandard spaces. *Electronic Journal of Statistics* 16(2), 4679–4741.

Severn, K. E., I. L. Dryden, and S. P. Preston (2021). Non-parametric regression for networks. *Stat* 10(1), e373.

Severn, K. E., I. L. Dryden, and S. P. Preston (2022). Manifold valued data analysis of samples of networks, with applications in corpus linguistics. *The Annals of Applied Statistics* 16(1), 368–390.

Shi, X., M. Styner, J. Lieberman, J. G. Ibrahim, W. Lin, and H. Zhu (2009). Intrinsic regression models for manifold-valued data. In *Medical Image Computing and Computer-Assisted Intervention–MICCAI 2009*, pp. 192–199. Springer.

Song, D. and K. Han (2023). Errors-in-variables Fréchet regression with low-rank covariate approximation. In *Advances in Neural Information Processing Systems*, Volume 36, pp. 80575–80607.

Srivastava, A., I. Jermyn, and S. Joshi (2007). Riemannian analysis of probability density functions with applications in vision. In *2007 IEEE Conference on Computer Vision and Pattern Recognition*, pp. 1–8. IEEE.

Sturm, K.-T. (2003). Probability measures on metric spaces of nonpositive curvature. *Heat*

Kernels and Analysis on Manifolds, Graphs, and Metric Spaces (Paris, 2002) 338, 357–390.

Sun, L., Z. Huang, Q. Wan, H. Peng, and P. S. Yu (2024). Spiking graph neural network on Riemannian manifolds. *Advances in Neural Information Processing Systems* 37, 34025–34055.

Szabó, Z., B. K. Sriperumbudur, B. Póczos, and A. Gretton (2016). Learning theory for distribution regression. *Journal of Machine Learning Research* 17(1), 5272–5311.

Turnbaugh, P. J., M. Hamady, T. Yatsunenko, B. L. Cantarel, A. Duncan, R. E. Ley, M. L. Sogin, W. J. Jones, B. A. Roe, J. P. Affourtit, et al. (2009). A core gut microbiome in obese and lean twins. *Nature* 457(7228), 480–484.

van den Boogaart, K. G., J. J. Egozcue, and V. Pawlowsky-Glahn (2014). Bayes Hilbert spaces. *Australian & New Zealand Journal of Statistics* 56(2), 171–194.

Villani, C. (2008). *Optimal Transport: Old and New*, Volume 338. Springer Science & Business Media.

Virta, J., K.-Y. Lee, and L. Li (2022). Sliced inverse regression in metric spaces. *Statistica Sinica* 32, 2315–2337.

Weng, J., K. Tan, C. Wang, and Z. Yu (2025). Sparse Fréchet sufficient dimension reduction with graphical structure among predictors. *Scandinavian Journal of Statistics* 52(3), 1422–1443.

Xu, H. and H. Li (2025). Wasserstein F-tests for Fréchet regression on Bures–Wasserstein manifolds. *Journal of Machine Learning Research* 26(77), 1–123.

Yan, X., X. Zhang, and P. Zhao (2024). Frequentist model averaging for global Fréchet regression. *IEEE Transactions on Information Theory* 71(3), 1994–2006.

Ying, C. and Z. Yu (2022). Fréchet sufficient dimension reduction for random objects. *Biometrika* 109(4), 975–992.

Ying, C., Z. Yu, and X. Zhang (2025). Distance weighted directional regression for Fréchet sufficient dimension reduction. *Biometrics* 81(2), ujaf051.

Yuan, Y., H. Zhu, W. Lin, and J. Marron (2012). Local polynomial regression for symmetric positive definite matrices. *Journal of the Royal Statistical Society: Series B (Statistical Methodology)* 74, 697–719.

Zemel, Y. and V. M. Panaretos (2019). Fréchet means and Procrustes analysis in Wasserstein space. *Bernoulli* 25(2), 932–976.

Zhang, C., P. Kokoszka, and A. Petersen (2022). Wasserstein autoregressive models for density time series. *Journal of Time Series Analysis* 43(1), 30–52.

Zhang, Q., L. Xue, and B. Li (2024). Dimension reduction for Fréchet regression. *Journal of the American Statistical Association* 119(548), 2733–2747.

Zhou, Y., S. I. Iao, and H.-G. Müller (2025a). End-to-end deep learning for predicting metric space-valued outputs. *arXiv preprint arXiv:2509.23544*.

Zhou, Y., S. I. Iao, and H.-G. Müller (2025b). Fréchet geodesic boosting. In *Advances in Neural Information Processing Systems*. (in press).

Zhou, Y. and H.-G. Müller (2022). Network regression with graph Laplacians. *Journal of Machine Learning Research* 23(320), 1–41.

Zhou, Y. and H.-G. Müller (2024). Wasserstein regression with empirical measures and density estimation for sparse data. *Biometrics* 80(4), ujae127.

Zhou, Y., H.-G. Müller, C. Zhu, Y. Chen, J.-L. Wang, J. O’Muircheartaigh, M. Bruchhage,

S. Deoni, and R. Consortium (2023). Network evolution of regional brain volumes in young children reflects neurocognitive scores and mother’s education. *Scientific Reports* 13(1), 2984.

Zhu, C. and H.-G. Müller (2023). Autoregressive optimal transport models. *Journal of the Royal Statistical Society Series B: Statistical Methodology* 85(3), 1012–1033.

Zhu, C. and H.-G. Müller (2024). Spherical autoregressive models, with application to distributional and compositional time series. *Journal of Econometrics* 239(2), 105389.

Zhu, H., Y. Chen, J. G. Ibrahim, Y. Li, C. Hall, and W. Lin (2009). Intrinsic regression models for positive-definite matrices with applications to diffusion tensor imaging. *Journal of the American Statistical Association* 104(487), 1203–1212.

A Choices of Hyperparameters for DFNN

A.1 Choices of Architectural and Regularization-related Hyperparameters for DFNN

For the proposed DFNN method, the grids of candidate values for each architectural and regularization-related hyperparameters for each experiment are listed in Tables 7–9, and the selected values via grid search for each experiment are listed in Table 10.

Table 7: Grids of architectural and regularization-related hyperparameters in Experiment 1.

Hyperparameter	Values
Hidden sizes $\{p_l\}_{l=1}^{L-1}$	512, 1024, 2048
Hidden size p_L	8, 16, 24
Hidden width L	3, 4
LR	0.001, 0.005, 0.01
DR	0.1, 0.2, 0.3

Table 8: Grids of architectural and regularization-related hyperparameters in Experiment 2.

Hyperparameter	Values
Hidden sizes $\{p_l\}_{l=1}^{L-1}$	256, 512, 1024, 4096
Hidden size p_L	5, 10, 15
Hidden width L	3, 4
LR	0.001, 0.01, 0.1
DR	0.1, 0.2, 0.3

A.2 Choices of Hyperparameters Used in the Early Stopping Rule

For each case in the experiments, we select the values of the hyperparameters, N_{initial} , $\delta_{\text{tolerance}}$, and N_{patience} , used in the early stopping rule stated in Section 4.1, via a grid

Table 9: Grids of architectural and regularization-related hyperparameters in Experiment 3.

Hyperparameter	Values
Hidden sizes $\{p_l\}_{l=1}^{L-1}$	128, 256, 512, 1024
Hidden size p_L	7, 14, 21
Hidden width L	3, 4
LR	0.001, 0.01, 0.01
DR	0.1, 0.2, 0.3

Table 10: Architectural and regularization-related hyperparameters for DFNN.

Experiment	Hidden sizes $\{p_l\}_{l=1}^{L-1}$	Hidden width L	Hidden size p_L	LR	DR
Experiment 1	2048	4	8	0.001	0.3
Experiment 2	4096	4	15	0.01	0.3
Experiment 3	1024	4	14	0.01	0.3

search and then use the corresponding choices for the experiment. The values selected for each experiment are listed in Table 11.

Table 11: Early-stopping hyperparameters used in the experiments.

Experiment	N_{initial}	$\delta_{\text{tolerance}}$	N_{patience}
Experiment 1	50	1.0×10^{-5}	150
Experiment 2	50	1.0×10^{-5}	100
Experiment 3	500	1.0×10^{-5}	1000

B Other Details of the Experiments

B.1 Implementations of Other Methods

For SDR and DFR, we follow the implementations in [Iao et al. \(2025\)](#). Specifically, local Fréchet regression is applied with a Gaussian kernel and bandwidth given by 10% of the empirical range of each input variable. The hyperparameters of DFR used in each setting are summarized in Table 12.

Table 12: Architectural and regularization-related hyperparameters for DFR.

Experiment	Hidden sizes $\{p_l\}_{l=1}^{L-1}$	Hidden width L	Hidden size p_L	LR	DR
Experiment 1	64	4	2	0.0005	0.3
Experiment 2	32	4	2	0.0005	0.3

B.2 U.S. States' Employment Occupational Compositions Used in Experiment 3

State-level employment composition data was collected from the Federal Reserve Economic Data (FRED), publicly available at <https://fred.stlouisfed.org/>.